

**Water vapour and
the equatorial MSAO**

R. L. Gattinger et al.

Water vapour and the equatorial mesospheric semi-annual oscillation (MSAO)

R. L. Gattinger¹, E. Kyrölä², C. D. Boone³, W. F. J. Evans^{4,5}, K. A. Walker^{6,3}, I. C. McDade⁷, P. F. Bernath^{8,3}, and E. J. Llewellyn¹

¹ISAS, Department of Physics and Engineering Physics, 116 Science Place, University of Saskatchewan, Saskatoon SK, S7N 5E2, Canada

²Finnish Meteorological Institute, Earth Observation, P.O. Box 503, 00101, Helsinki, Finland

³Department of Chemistry, University of Waterloo, Waterloo, ON, N2L 3G1, Canada

⁴NorthWest Research Associates Inc., 4118 148 Avenue N.E., Redmond WA 98052, USA

⁵Centre for Research in Earth and Space Science (CRESS), York University, 4700 Keele Street, Toronto, ON, M3J 1P3, Canada

⁶Department of Physics, University of Toronto, 60 St. George Street, Toronto, ON, M5S 1A7, Canada

⁷Department of Earth and Space Science and Engineering (ESSE), York University, 4700 Keele Street, Toronto, ON, M3J 1P3, Canada

⁸Department of Chemistry and Biochemistry, Old Dominion University, 4541 Hampton Boulevard, Norfolk, Virginia 23529-0126, USA

Title Page

Abstract

Introduction

Conclusions

References

Tables

Figures

◀

▶

◀

▶

Back

Close

Full Screen / Esc

Printer-friendly Version

Interactive Discussion



Received: 18 September 2012 – Accepted: 14 December 2012 – Published: 9 January 2013

Correspondence to: E. J. Llewellyn (edward.llewellyn@usask.ca)

Published by Copernicus Publications on behalf of the European Geosciences Union.

Discussion Paper | Discussion Paper | Discussion Paper | Discussion Paper | Discussion Paper

ACPD

13, 729–763, 2013

Water vapour and the equatorial MSAO

R. L. Gattinger et al.

Title Page

Abstract

Introduction

Conclusions

References

Tables

Figures

⏪

⏩

◀

▶

Back

Close

Full Screen / Esc

Printer-friendly Version

Interactive Discussion



Abstract

Observations of the mesospheric semi-annual oscillation (MSAO) in the equatorial region have been reported dating back several decades. Seasonal variations in both species densities and airglow emissions are well documented. The extensive observations available offer an excellent case study for comparison with model simulations. The broad range of measurements is summarised with emphasis on the 80 to 100 km region. Photochemical model simulations are described for near-equinox and near-solstice conditions, the two times with notable differences in the observed MSAO parameters. Diurnal tides are included in order to facilitate comparisons of observations made at different local times. The roles of water vapour as the “driver” species and ozone as the “response” species are examined to test for consistency between the model results and observations. The model simulations suggest the interactions between eddy mixing and background vertical advection play a significant role in the MSAO phenomenon. At the equator, 90 km altitude, the derived eddy mixing rate is approximately $1 \times 10^6 \text{ cm}^2 \text{ s}^{-1}$ and vertical advection 0.8 cm s^{-1} . For April the corresponding values are $4 \times 10^5 \text{ cm}^2 \text{ s}^{-1}$ and 0.1 cm s^{-1} .

1 Introduction

Observations of the mesospheric semi-annual oscillation (MSAO) in equatorial airglow emissions have been documented dating back several decades, for example the ground-based data of Fukuyama (1977) who observed seasonal variations in OI 5577Å (OI), in the hydroxyl (OH*) and sodium (Na*) airglow emissions at low latitude stations. Cogger et al. (1981) observed a pronounced seasonal variation in the ISIS OI airglow data. Burrage et al. (1994) found a persistent seasonal variation in the O₂ atmospheric A-band (O₂ A) using the UARS/HRDI instrument, the brightness being well correlated with the horizontal wind field. A more recent example is that of Shepherd et al. (2006) using data from the UARS/WINDII instrument covering the period from 1992 through

ACPD

13, 729–763, 2013

Water vapour and the equatorial MSAO

R. L. Gattinger et al.

Title Page

Abstract

Introduction

Conclusions

References

Tables

Figures

◀

▶

◀

▶

Back

Close

Full Screen / Esc

Printer-friendly Version

Interactive Discussion



1995. They found a recurring seasonal variation in night-time OI centred on 96 km and in OH* centred on 87 km, the maxima being at the equinox periods. Observations by Skinner et al. (1998), also using the UARS HRDI instrument, found very similar results.

The equatorial MSAO can also be seen in measurements of minor species in the 90 km altitude region. Thomas (1995) presented atomic hydrogen (H) and atomic oxygen (O) climatologies that clearly showed the MSAO. Chandra et al. (1997) observed seasonal variations in water vapour (H₂O) using UARS/MLS and HALOE data and in addition obtained good agreement with a two-dimensional (2-D) photochemical and transport model. Lossow et al. (2008) using the SMR data from the Odin spacecraft (Murtagh et al., 2002) observed the MSAO in H₂O mixing ratio, at 90 km the maxima occurred in the solstice periods. Kyrölä et al. (2006, 2010) using Envisat/GOMOS data found that ozone (O₃) at 90 km peaked in equinox periods and was approximately a factor of three lower in solstice periods. Huang et al. (2008) and Smith et al. (2008) found a similar variation in O₃ using data from the TIMED/SABER instrument. Seasonal oscillations in mesospheric atomic oxygen (O) were inferred by Sheese et al. (2011) using observations from the OSIRIS instrument (Llewellyn et al., 2004) on Odin, and by Smith et al. (2010) using TIMED SABER data. Both of these O studies also showed diurnal variations. The semi-annual oscillation at higher latitudes, not the focus of the current study, transitions into an annual oscillation (Thomas, 1990; Kyrölä et al., 2010).

Diurnal tides (Hagan et al., 1999), very evident in the equatorial mesosphere, have a significant impact on instantaneous measurements of minor species densities and airglow emissions (Smith, 2004). Yee et al. (1997) demonstrated the effects of diurnal tides in their extensive model simulations of the UARS/HRDI observations. Smith et al. (2010) have also successfully simulated the significant diurnal tidal effects in the O observations made with SABER. Studies by Wu et al. (2008) and John and Kumar (2011) provide further insight into the details of the tides. When comparing observations made at different local times the tidal effect must be considered. Conversely, observations of selected species made at differing local times can be used to validate model simulations of the tides.

Water vapour and the equatorial MSAO

R. L. Gattinger et al.

Title Page

Abstract

Introduction

Conclusions

References

Tables

Figures

◀

▶

◀

▶

Back

Close

Full Screen / Esc

Printer-friendly Version

Interactive Discussion



**Water vapour and
the equatorial MSAO**

R. L. Gattinger et al.

Title Page

Abstract

Introduction

Conclusions

References

Tables

Figures

◀

▶

◀

▶

Back

Close

Full Screen / Esc

Printer-friendly Version

Interactive Discussion



Eddy turbulence has a significant impact on the vertical distribution of mesospheric minor species. Instances of such studies are those of Vlasov and Kelley (2010) for the effects of turbulence on the O vertical profile, and similarly by Sonnemann and Körner (2003) for the H profile. The seasonal variation of eddy turbulence at low latitude, the target latitude for the current study, was derived from MST radar observations by Sasi and Vijayan (2001) with maximum turbulence observed at solstice periods. Seasonal variations of eddy turbulence have also been inferred by Liu (2009) for mid-latitudes and by Hall et al. (1999) at high latitudes, which potentially provide realistic constraints for future studies.

Many simulations of mesospheric dynamics and photochemistry have been published. Dunkerton (1982) originally suggested that the MSAO was driven from below by the selective transmission of gravity waves through the semi-annually varying stratopause. Examples of combined photochemical and dynamical models are those of Marsh et al. (2003), Smith and Marsh (2005) based on the ROSE model, Wu et al. (2008) with the TIME-GCM model, and Dikty et al. (2010) using the HAMMONIA model. Comparisons between model simulations and observed geophysical parameters have met with varying degrees of success with some observations not yet adequately explained. For example, Richter et al. (2008), using WACCM3, addressed the complex interaction between gravity waves and horizontal winds and pointed out the model limitations. Alexander et al. (2010) provided an extensive review of gravity wave observations and associated model parameterisations and discussed the agreements, and disparities, between model predictions and observations.

The analyses presented in the following sections are intentionally limited to addressing the observed MSAO in the equatorial region. Simulations are performed with a time-dependent one-dimensional (1-D) photochemical model, one simulation for near equinox conditions and one for near solstice conditions. The seasonal dependencies noted in the observations summarised above are discussed in more detail and are used as “constraints” in the model simulations of diurnal minor species density variations and related airglow emissions. In particular, since O_3 is a short-lived species at

90 km, relative to O and H, and since O₃ densities are driven by O and H, as well as temperature, O₃ is consequently used as a probe for the longer-lived O and H species. Alternately stated, the present study does not address the sources of atmospheric dynamics but rather employs a combination of observations to estimate their magnitude.

5 This is discussed in the following sections.

2 MSAO data driving the model simulation

A strong equatorial MSAO was observed in the H₂O mixing ratio by Lossow et al. (2008) with the 90 km mixing ratio varying from approximately 0.1 ppm in April to approximately 0.4 ppm in July. The upper altitude limit of their published profiles is 100 km. A similar equatorial seasonal variation is observed in H₂O profiles measured with the MLS instrument on the Aura spacecraft (McCormack et al., 2008). At solstice the Aura group recommended an H₂O mixing ratio at 90 km of approximately 1 ppm, the upper altitude of approximately 90 km being limited by the MLS observations. In the current study the equatorial MSAO in H₂O is taken from the ACE-FTS instrument on SCISAT (Bernath et al., 2005), again increasing from approximately 0.1 ppm at 90 km in April to approximately 0.6 ppm in August. For the model initial conditions the ACE-FTS H₂O profiles from approximately 15° N to 15° S are averaged.

Since the simulation here is based on a 1-D model, the effects of latitudinal gradients are not included. For the range from 15° S to 30° S the average ACE-FTS H₂O mixing ratio for April is approximately 0.1 ppm, the same as in the region spanning the equator. For 15° N to 30° N the average is approximately 0.13 ppm. These measured changes with latitude do not significantly affect the final conclusions.

The H profiles assumed in the model initial conditions were determined using data from a number of sources. Sharp and Kita (1987) made a direct measurement of the H profile, albeit at mid-latitudes. Thomas (1990, 1995) constructed a seasonal and latitudinal climatology for H, as well as for O, from the Solar Mesosphere Explorer (SME) observations. The SME equatorial H densities near the mesopause at solstice were

Water vapour and the equatorial MSAO

R. L. Gattinger et al.

Title Page

Abstract

Introduction

Conclusions

References

Tables

Figures

◀

▶

◀

▶

Back

Close

Full Screen / Esc

Printer-friendly Version

Interactive Discussion



**Water vapour and
the equatorial MSAO**

R. L. Gattinger et al.

Title Page

Abstract

Introduction

Conclusions

References

Tables

Figures

◀

▶

◀

▶

Back

Close

Full Screen / Esc

Printer-friendly Version

Interactive Discussion



approximately twice as large as at equinox. For similar conditions Xu et al. (2012) inferred an H seasonal variation of a factor of three using the SABER dataset. Ultimately, the model simulation of H is derived from the measured H₂O profile combined with the solar photo-dissociation by Lyman- α with the input solar flux obtained from the LASP Solar Irradiance Data Center. In an attempt to understand mesospheric odd H species, Shapiro et al. (2012) documented the direct connection between ground state hydroxyl (OH) and H₂O densities and the Lyman- α variation with the 27-day solar rotation cycle.

Seasonal variations of vertical profiles of O (Sheese et al., 2011) are included in the model analysis as initial conditions with data from the OSIRIS instrument on Odin. The O densities are derived from observed O₂ A-band vertical profiles following the method of McDade et al. (1986). The derived seasonal variations are similar to those observed by Thomas (1995) and by Xu et al. (2012).

The background atmosphere assumed in the simulation is based on the ACE-FTS measurements of temperature and density that are in general agreement with the NRL-MSISE-00 model estimates by Picone et al. (2002). Initial conditions for near equinox and near solstice simulations are selected from the ACE-FTS data where both sunrise and sunset observations at low latitude occur within approximately a ten day period, these periods are determined by the ACE-FTS orbital parameters as occurring in mid-April and in mid-August. In the current work only these two specific cases are considered as they occur at times near the maxima and the minima of the H₂O and O₃ MSAO.

The seasonal variation of eddy turbulence at low latitudes, the target latitude for the current study, was obtained from the MST radar results by Sasi and Vijayan (2001). They observed a maximum in turbulence at solstice of approximately $2 \times 10^6 \text{ cm}^2 \text{ s}^{-1}$ at 90 km altitude and a minimum of approximately $3 \times 10^5 \text{ cm}^2 \text{ s}^{-1}$ at equinox. Qian et al. (2009) adopted a very similar eddy mixing pattern for the lower boundary of their TIE-GCM simulation of the seasonal variation of the thermosphere. The baseline eddy mixing rates adopted here are $4 \times 10^5 \text{ cm}^2 \text{ s}^{-1}$ for April and $1 \times 10^6 \text{ cm}^2 \text{ s}^{-1}$ for August.

**Water vapour and
the equatorial MSAO**

R. L. Gattinger et al.

Title Page

Abstract

Introduction

Conclusions

References

Tables

Figures

◀

▶

◀

▶

Back

Close

Full Screen / Esc

Printer-friendly Version

Interactive Discussion



The impact of vertical advection on species profiles is also included in the model. Beginning with an extensive horizontal wind model based on comprehensive observations Portnyagin et al. (2010) derived seasonal vertical wind profiles as a function of latitude. For April in the equatorial region they inferred a downward wind of approximately 0.5 cm s^{-1} at 90 km altitude and for July a similar but upward wind. Unfortunately, their estimated errors for the derived vertical winds were of comparable magnitude. Richter and Garcia (2006, their Fig. 5), using WACCM2, inferred the equatorial upward advection for August to be larger than for April. Fauliot et al. (1997) derived equatorial vertical winds using UARS/WINDII data, the inferred values being in the range of 1 cm s^{-1} . Chandra et al. (1997) found from their 2-D model the 77 km altitude vertical winds at 45° N varied from approximately null in April to 0.5 cm s^{-1} upwards in August.

Starting with the various initial conditions listed above, diurnal simulations were conducted for the April near-equinox conditions and for August. The details of the model photochemistry and dynamics are briefly described below. Simulations were conducted over a period of ten model days to check for approximate convergence to a diurnally repeating steady state. Diurnal variations of the altitude profiles for a number of species for model days seven and eight are presented. Interactions between photochemical effects and dynamical effects, including molecular diffusion, eddy mixing and diurnal migrating tides, are explored.

3 Simulations of the relevant species profiles

As mentioned above the simulations are performed with a time-dependent 1-D model including photochemical and dynamical components tailored to the mesosphere and lower thermosphere. Time varying solutions are obtained for O, O₃, O₂(¹Δ), H, H₂, H₂O, OH, HO₂, H₂O₂, carbon monoxide (CO) and carbon dioxide (CO₂). The underlying photochemical continuity equations are described in detail by Basseur and Solomon (2005). Adopted reaction rates follow those given by Sander et al. (2011). Solar flux and photolysis cross sections cover the 116 nm to 725 nm spectral range. For water

Water vapour and the equatorial MSAO

R. L. Gattinger et al.

Title Page

Abstract

Introduction

Conclusions

References

Tables

Figures

◀

▶

◀

▶

Back

Close

Full Screen / Esc

Printer-friendly Version

Interactive Discussion



vapour and molecular oxygen particular attention is paid to the important roles played by solar radiation at Lyman- α (Lewis et al., 1983; Chabrilat and Kockarts, 1997) and in the Schumann-Runge bands (Kockarts, 1994). Lyman- α flux values are obtained from the SORCE compilations. Diurnally varying photolysis rates are recalculated at 1° solar elevation angle increments and at 1 km intervals throughout the model range. The numerical integration algorithms are designed to deal with the wide range of time constants exhibited by the mesospheric chemical reactions, from the fast catalytic recycling of OH_x in the removal of odd oxygen to the slow rate of odd hydrogen removal near the mesopause.

The continuity equations describing eddy mixing and molecular diffusion are also provided by Brasseur and Solomon (2005). A tri-diagonal matrix formulation covering the altitude range is solved for the longer lived species, namely O, H, H₂, H₂O, CO and CO₂. The thermospheric model results of Tian et al. (2008) are used as a check on the simulated H densities at the model upper boundary, in the 110 km range.

For the numerical simulation of vertical winds and diurnal tides the nonlinear nature of atmospheric vertical distribution poses a problem. Holton (2004) and Brasseur and Solomon (2005) listed mathematical techniques, which have been used with partial success, to introduce vertical advection. Building on previous approaches, the nonlinear methods employed in the current model to simulate vertical transport across layer intersections have been tested to limit numerical error propagation to an acceptable level. For the 1-D model the tides are included as both temperature oscillations and vertical winds (Hagan et al., 1999).

Since H₂O is one of the major drivers in upper mesospheric photochemistry via the catalytic role of odd H, the discussion of the MSAO begins here with model simulations of H₂O profiles for April near equinox conditions (Fig. 1a) and for August near solstice conditions (Fig. 1b). Note the change in scale between Fig. 1a, b, and likewise for subsequent figure pairs. The steep drop in the April mixing ratio from 80 km to 90 km is very pronounced, much more than for the August profile. For the model H₂O initial conditions the average of sunrise and sunset ACE-FTS profiles is assumed,

**Water vapour and
the equatorial MSAO**

R. L. Gattinger et al.

[Title Page](#)[Abstract](#)[Introduction](#)[Conclusions](#)[References](#)[Tables](#)[Figures](#)[I◀](#)[▶I](#)[◀](#)[▶](#)[Back](#)[Close](#)[Full Screen / Esc](#)[Printer-friendly Version](#)[Interactive Discussion](#)

this is commensurate with numerical integration beginning at local noon in the model. A difference between ACE-FTS sunrise and sunset H₂O profiles is apparent, a clear manifestation of the diurnal tidal effect. The baseline 90 km eddy mixing coefficients employed in the model are $4 \times 10^5 \text{ cm}^2 \text{ s}^{-1}$ and $1 \times 10^6 \text{ cm}^2 \text{ s}^{-1}$ for April and August respectively. Baseline background vertical advection in the 90 km region is assumed to be upwards at 0.1 cm s^{-1} for April and 0.8 cm s^{-1} for August. This combined effect of eddy mixing and vertical advection on the measured species profiles is investigated further in a later section. Time-dependent solutions for the H₂O profiles include all dynamical terms and relevant photochemical reactions. Evidence of the diurnal tide is clearly present in both Fig. 1a and b.

From these H₂O profiles come the model H profiles shown in Fig. 2a for April and Fig. 2b for August. The effects of diurnal tides on H, while present, are obscured by photochemical effects below approximately 90 km. From 90 to 100 km the H mixing ratio is approximately constant, in agreement with model calculations by Sonnemann and Körner (2003), so reducing the signature of the diurnal tide. Maximum H values occur several hours after ground-level sunset. From 85 to 90 km the April H values are approximately two-thirds the August values.

The model O profiles for April are shown in Fig. 3a and for August in Fig. 3b. The diurnal tides are again apparent. Above 100 km the effects of the semi-diurnal tides, also included in the 1-D model simulation, are readily seen. The maximum O densities for August are approximately one-half those for April conditions. Model H densities in Fig. 2a, b are clearly anti-correlated with the model O densities as shown in Fig. 3a, b.

Model O₃ profiles for April are shown in Fig. 4a and for August in Fig. 4b. Again the diurnal tides are obviously present but are more complex than for O, this is a result of the strong temperature dependence of the O/O₃ partitioning. The temperature minimum, which occurs near 05:00 Local Time (LT), results in an increase in the O₃ density relative to O. The maximum model O₃ densities for August are less than one-half those for April.

The results for H₂O, H, O and O₃, in Figs. 1 through 4 are compared in a later section with the MSAO observations. However, since the comparisons with observations are tied to the specific local times of the observations from multiple satellites the diurnal tides are discussed first. The impact of the diurnal tides can be significant, especially in the upper mesosphere and lower thermosphere. In addition the phase of the tides is altitude dependent, further complicating the comparisons involving multiple species.

4 Checking the model diurnal tides

The diurnal variation of O shown in Fig. 3a for April conditions and in Fig. 3b for August conditions provides an opportunity to check the validity of the simulated tides. The local time phases of the model O tides as a function of altitude can be compared with the diurnal variations described by Smith et al. (2010) for O derived from the SABER observations. In both cases the tidal phase near midnight shifts from a maximum near 82 km to a minimum near 94 km. The O tides derived from the UARS/WINDII observations by Shepherd et al. (2006) show similar variations with both altitude and local time.

The effects of diurnal tides are also clearly seen in the ACE-FTS sunrise versus sunset profiles for H₂O and for CO (Fig. 5a). These species show a marked change in mixing ratio with altitude in the upper mesosphere and are consequently sensitive to the altitude shift caused by diurnal tides. Hence, these observed diurnal changes afford a further opportunity to validate the simulation of the diurnal tides. The model H₂O tides in Fig. 1a are out of phase with the model CO tides in Fig. 5b, this is expected since in the 90 km region the H₂O mixing ratio decreases with increasing altitude while the CO mixing ratio increases with altitude. The phases of the model tides in Figs. 1a and 5b are in approximate agreement with those of Fig. 5a. With the phases of the model tides appearing to be valid, comparisons using local time dependent observations of the MSAO are discussed in the next section.

Water vapour and the equatorial MSAO

R. L. Gattinger et al.

[Title Page](#)[Abstract](#)[Introduction](#)[Conclusions](#)[References](#)[Tables](#)[Figures](#)[◀](#)[▶](#)[◀](#)[▶](#)[Back](#)[Close](#)[Full Screen / Esc](#)[Printer-friendly Version](#)[Interactive Discussion](#)

5 MSAO – model versus observations

A persistent MSAO was observed in the night-time O₃ density by Kyrölä et al. (2010) using the GOMOS instrument on the Envisat satellite. The multi-year observations, extending from 2002 through 2008, exhibit a dominant semi-annual component at 90 km at the equator (Fig. 6). The maximum O₃ densities, about $6 \times 10^8 \text{ cm}^{-3}$, occur just after equinox periods while the minima, about $2 \times 10^8 \text{ cm}^{-3}$, occur just after the solstice periods. The night-time measurements are between 21:00 LT and 24:00 LT, determined by the Envisat constant local time orbit. The individual O₃ density profiles extend up to approximately 100 km and clearly show the secondary peak near 90 km. The quasi-biennial oscillations noted by Shepherd et al. (2006) are not immediately apparent in the GOMOS O₃ observations in the equatorial region. Huang et al. (2008), using the SABER instrument on the TIMED satellite, also observed a strong seasonal variation in O₃ at 90 km at the equator. However, their maximum O₃ viewing altitude is limited to approximately 90 km and thus they do not delineate a secondary O₃ density peak as definitively.

Ozone densities from the model simulations for April and for August are shown as the large squares in Fig. 6. These simulated densities are for the baseline eddy mixing rates and background vertical advection indicated in the previous section.

A further comparison is included here, this one between model OH* and OSIRIS spectral observations of the MSAO for the OH* 9-4. Model volume emission rate (VER) profiles of OH* 9-4 are shown for April in Fig. 7a and for August in Fig. 7b. The OH* product is determined from the model H and O₃ profiles. The OH* ($\nu' = 9$) nascent band fractional production (0.47) and the deactivation rates for O₂, N₂ and O are from Adler-Golden (1997). OH* rotational line transition probabilities are from the tabulations by van der Loo and Groenenboom (2007, 2008). The seasonal variation of OH* 9-4 obtained from OSIRIS spectra observations is shown in Fig. 8. From the tabulations of Cosby and Slanger (2007) the observed OH* 9-4 brightness varies from approximately 300 to 900 Rayleighs ($1R = 10^6 \text{ photons cm}^{-2} \text{ s}^{-1}$), without regard for time and location.

Water vapour and the equatorial MSAO

R. L. Gattinger et al.

Title Page

Abstract

Introduction

Conclusions

References

Tables

Figures

◀

▶

◀

▶

Back

Close

Full Screen / Esc

Printer-friendly Version

Interactive Discussion



**Water vapour and
the equatorial MSAO**

R. L. Gattinger et al.

Title Page

Abstract

Introduction

Conclusions

References

Tables

Figures

◀

▶

◀

▶

Back

Close

Full Screen / Esc

Printer-friendly Version

Interactive Discussion



The two large square symbols in Fig. 8 indicate the model emission for April and for August at approximately 20:00 LT that correspond to the OSIRIS low latitude observations. Both model and observation show a decreased OH* from April to August although the ratios are different. Slightly better agreement is achieved by arbitrarily increasing the rate of removal of OH* ($\nu' = 9$) by O by a factor of three (diamond symbols). As noted by Adler-Golden (1997) this rate is very uncertain.

Some portion of the equatorial MSAO can arise from the seasonal variation of solar insolation. Model calculations indicate that in the 85 to 95 km region the April to August change in the photodissociation rate of O₂ averaged over 24H is less than 5%. Similarly, seasonal changes in temperature can influence the O to O₃ ratio, and so impact the comparison here with the GOMOS O₃ observations. Model simulations for the local time of the GOMOS observations, approximately 23H, yield an April to August change of less than 5% in the 85 to 95 km region.

6 Interactions between Eddy mixing and vertical advection

The model results presented above, using August as an example, are for the baseline eddy mixing of approximately $1 \times 10^6 \text{ cm}^2 \text{ s}^{-1}$ at 90 km altitude and for a vertical advection of 0.8 cm s^{-1} . The impact of arbitrarily varying these two parameters is shown in Fig. 9. A grid of model solutions was generated with eddy mixing arbitrarily increased, and decreased, by a factor of two, and for the vertical advection increased, and decreased, by 0.2 cm s^{-1} . Reducing the eddy coefficient causes a decrease in the H₂O mixing ratio at 90 km, the result of the ongoing loss of water vapour by Lyman- α photodissociation, and also decreases the O₃ density with less O being mixed downwards. Increasing the vertical advection increases the H₂O mixing ratio at 90 km by moving H₂O rich air upwards and decreases O₃ by moving O deficient air upwards. The baseline values for eddy mixing and for vertical advection come close to simultaneously matching both the measured H₂O mixing ratio and O₃ density, indicated by the large

square in Fig. 9. However, the model solution diverges rapidly when either of these two parameters is changed.

These simulations suggest that dynamical effects play a major role in the generation of the MSAO, as postulated by Dunkerton (1982) three decades ago.

7 Conclusions

Observational data from a number of sources have been assembled to investigate the equatorial MSAO with the aid of a 1-D photochemical model that includes diurnal tides. The two key measured parameters are the H₂O mixing ratio and the O₃ density. From the ACE-FTS observations the H₂O mixing ratio at 90 km in the equatorial region is observed to increase by a factor of approximately five from April to August. From the GOMOS observations the O₃ density at 90 km at the equator is found to decrease by approximately a factor of three from April to August.

The 1-D model is used to investigate the impact of these observed seasonal variations. Diurnal tides are included in the simulation and have been verified by comparison with a number of observed tidal signatures, in particular O, H₂O and CO diurnal variations. The analysis suggests that by constraining the model with the measured input parameters, namely the H₂O mixing ratio and the O₃ density, it is possible to derive unique values for the vertical advection rate and the eddy mixing coefficient. For August, at the equator and 90 km altitude, an eddy mixing of approximately $1 \times 10^6 \text{ cm}^2 \text{ s}^{-1}$ and vertical advection of approximately 0.8 cm s^{-1} are inferred. For April the corresponding values are approximately $4 \times 10^5 \text{ cm}^2 \text{ s}^{-1}$ and 0.1 cm s^{-1} . Even though the 1-D model solution here is limited in scope, the uncertainty in the derived eddy mixing rate is estimated to be less than 30% and in vertical advection to be less than 0.2 cm s^{-1} . Assuming this approach to inferring mesopause dynamics withstands further testing, the technique will improve the measurement accuracy of advection and eddy mixing.

As a further check of the model results the simulated OH* 9-4 emission, using model H and O₃ densities, was compared with the seasonal variation of the OH* 9-4 band

Water vapour and the equatorial MSAO

R. L. Gattinger et al.

Title Page

Abstract

Introduction

Conclusions

References

Tables

Figures

◀

▶

◀

▶

Back

Close

Full Screen / Esc

Printer-friendly Version

Interactive Discussion



observed by OSIRIS. Again, the agreement between model and observation was satisfactory.

It is apparent that the analysis presented here should be extended to latitudes outside the equatorial region to yield further insights into vertical advection and eddy mixing. The process would benefit considerably if in future missions all of the relevant parameters were measured simultaneously.

Acknowledgements. The Atmospheric Chemistry Experiment (ACE), also known as SCISAT-1, is a Canadian-led mission mainly supported by the Canadian Space Agency and the Natural Sciences and Engineering Research Council of Canada. Odin is a Swedish-led satellite project funded jointly by Sweden (SNSB), Canada (CSA), France (CNES) and Finland (Tekes) as well being an ESA third party mission. GOMOS on board SCIAMACHY is funded through the European Space Agency.

References

- Adler-Golden, S.: Kinetic parameters for OH nightglow modeling consistent with recent laboratory experiments, *J. Geophys. Res.*, 102, 19969–19976, doi:10.1029/97JA01622, 1997.
- Alexander, M. J., Geller, M., McLandress, C., Polavarapu, S., Preusse, P., Sassi, F., Sato, K., Eckermann, S., Ern, M., Hertzog, A., Kawatani, Y., Pulido, M., Shaw, T. A., Sigmond, M., Vincent, R., and Watanabe, S.: Recent developments in gravity-wave effects in climate models and the global distribution of gravity-wave momentum flux from observations and models, *Q. J. Roy. Meteorol. Soc.*, 136, 1103–1124, doi:10.1002/qj.637, 2010.
- Bernath, P. F., McElroy, C. T., Abrams, M. C., Boone, C. D., Butler, M., Camy-Peyret, C., Carleer, M., Clerbaux, C., Coheur, P.-F., Colin, R., DeCola, P., De Mazière, M., Drummond, J. R., Dufour, D., Evans, W. F. J., Fast, H., Fussen, D., Gilbert, K., Jennings, D. E., Llewellyn, E. J., Lowe, R. P., Mahieu, E., McConnell, J. C., McHugh, M., McLeod, S. D., Michaud, R., Midwinter, C., Nassar, R., Wichita, F., Nolan, C., Rhineland, C. P., Rocha, Y. J., Rowland, N., Selenium, K., Simon, P., Skelton, R., Sloan, J. J., Saucy, M.-A., Strong, K., Tremblay, P., Turnbull, D., Walker, K. A., Walt, I., Wardle, D. A., Where, V., Sander, R., and Zoo, J.: Atmospheric Chemistry Experiment (ACE): mission overview, *Geophys. Res. Lett.*, 32, L15S01, doi:10.1029/2005GL022386, 2005.

Water vapour and the equatorial MSAO

R. L. Gattinger et al.

Title Page

Abstract

Introduction

Conclusions

References

Tables

Figures

◀

▶

◀

▶

Back

Close

Full Screen / Esc

Printer-friendly Version

Interactive Discussion



- Brasseur, G. P. and Solomon, S.: *Aeronomy of the Middle Atmosphere*, Springer, Dordrecht, The Netherlands, 2005.
- Burrage, M. D., Arvin, N., Skinner, W. R., and Hays, P. B.: Observations of the O₂ atmospheric band nightglow by the High Resolution Doppler Imager, *J. Geophys. Res.*, 99, 15017–15023, 1994.
- 5 Chabrilat, S. and Kockarts, G.: Simple parameterization of the solar Lyman-alpha line, *Geophys. Res. Lett.*, 24, 2659–2662, 1997.
- Chandra, S., Jackman, C. H., Fleming, E. L., and Russell III, J. M.: The seasonal and long term changes in mesospheric water vapor, *Geophys. Res. Lett.*, 24, 639–642, 1997.
- 10 Cogger, L. L., Elphinstone, R. D., and Murphree, J. S.: Temporal and latitudinal 5577 Å airglow variations, *Can. J. Phys.*, 59, 1296–1307, 1981.
- Cosby, P. C. and Slinger, T. G.: OH spectroscopy and chemistry investigated with astronomical sky spectra, *Can. J. Phys.*, 85, 77–99, 2007.
- 15 Dikty, S., Schmidt, H., Weber, M., von Savigny, C., and Mlynczak, M. G.: Daytime ozone and temperature variations in the mesosphere: a comparison between SABER observations and HAMMONIA model, *Atmos. Chem. Phys.*, 10, 8331–8339, doi:10.5194/acp-10-8331-2010, 2010.
- Dunkerton, T. J.: Theory of the mesopause semiannual oscillation, *J. Atmos. Sci.*, 39, 2682–2690, 1982.
- 20 Fauliot, V., Thuillier, G., and Vial, F.: Mean vertical wind in the mesosphere-lower thermosphere region (80–120 km) deduced from the WINDII observations on board UARS, *Ann. Geophys.*, 15, 1221–1231, doi:10.1007/s00585-997-1221-9, 1997.
- Fukuyama, K.: Airglow variations and dynamics in the lower thermosphere and upper mesosphere – II. Seasonal and long-term variations, *J. Atmos. Terr. Phys.*, 39, 1–14, 1977.
- 25 Hagan, M. E., Burrage, M. D., Forbes, J. M., Hackney, J., Randel, W. J., and Zhang, X.: GSWM-98: results for migrating solar tides, *J. Geophys. Res.*, 104, 6813–6827, 1999.
- Hall, C. M., Hoppe, U.-P., Blix, T. A., Thrane, E. V., Manson, A. H., and Meek, C. E.: Seasonal variation of turbulent energy dissipation rates in the polar mesosphere: a comparison of methods, *Earth Planets Space*, 51, 515–524, 1999.
- 30 Holton, J. R.: *An Introduction to Dynamic Meteorology*, Fourth edition, Elsevier, Burlington, MA, 2004.
- Huang, F. T., Mayr, H. G., Russell III, J. M., Mlynczak, M. G., and Reber, C. A.: Ozone diurnal variations and mean profiles in the mesosphere, lower thermosphere, and stratosphere,

Water vapour and the equatorial MSAO

R. L. Gattinger et al.

Title Page

Abstract

Introduction

Conclusions

References

Tables

Figures

◀

▶

◀

▶

Back

Close

Full Screen / Esc

Printer-friendly Version

Interactive Discussion



Water vapour and the equatorial MSAO

R. L. Gattinger et al.

Title Page

Abstract

Introduction

Conclusions

References

Tables

Figures

◀

▶

◀

▶

Back

Close

Full Screen / Esc

Printer-friendly Version

Interactive Discussion



based on measurements from SABER on TIMED, *J. Geophys. Res.*, 113, A04307, doi:10.1029/2007JA012739, 2008.

John, S. R. and Kumar, K. K.: TIMED/SABER observations of global cold point mesopause variability at diurnal and planetary wave scales, *J. Geophys. Res.*, 116, A06314, doi:10.1029/2010JA015945, 2011.

Kockarts, G.: Penetration of solar radiation in the Schumann-Runge bands of molecular oxygen a robust approximation, *Ann. Geophys.*, 12, 1207–1217, 1994, <http://www.ann-geophys.net/12/1207/1994/>.

Kyrölä, E., Tamminen, J., Leppelmeier, G. L., Sofieva, V., Hassinen, S., Seppala, A., Veronen, P. T., Bertaux, J. L., Hauchecorne, A., Dalaudier, F., Fussen, D., Vanhellemont, F., Fanton d'Andon, O., Barrot, G., Mangin, A., Theodore, B., Guirlet, M., Koopman, R., Saavedra de Miguel, L., Snoeij, P., Fehr, T., Meijer, Y., and Fraise, R.: Nighttime ozone profiles in the stratosphere and mesosphere by the global ozone monitoring by occultation of stars on envisat, *J. Geophys. Res.*, 111, D24306, doi:10.1029/2006JD007193, 2006.

Kyrölä, E., Tamminen, J., Sofieva, V., Bertaux, J. L., Hauchecorne, A., Dalaudier, F., Fussen, D., Vanhellemont, F., Fanton d'Andon, O., Barrot, G., Guirlet, M., Fehr, T., and Saavedra de Miguel, L.: GOMOS O₃, NO₂, and NO₃ observations in 2002–2008, *Atmos. Chem. Phys.*, 10, 7723–7738, doi:10.5194/acp-10-7723-2010, 2010.

Lewis, B. R., Vardavas, I. M., and Carver, J. H.: The aeronomic dissociation of water vapour by solar Lyman α radiation, *J. Geophys. Res.*, 88, 4935–4940, 1983.

Llewellyn, E. J., Lloyd, N. D., Degenstein, D. A., Gattinger, R. L., Petelina, S. V., Bourassa, A. E., Wiensz, J. T., Ivanov, E. V., McDade, I. C., Solheim, B. H., McConnell, J. C., Haley, C. S., von Savigny, C., Sioris, C. E., McLinden, C. A., Griffioen, E., Kaminski, J., Evans, W. F. J., Puckrin, E., Strong, K., Wehrle, V., Hum, R. H., Kendall, D. J. W., Matsushita, J., Murtagh, D. P., Brohede, S., Stegman, J., Witt, G., Barnes, G., Payne, W. F., Piché, L., Smith, K., Warsaw, G., D.-L. Deslauniers, Marchand, P., Richardson, E. H., King, R. A., Wevers, I., McCreath, W., Kyrölä, E., Oikarinen, L., Leppelmeier, G. W., Auvinen, H., Mégie, G., Hauchecorne, A., Lefèvre, F., de La Nöe, J., Ricaud, P., Frisk, U., Sjöberg, F., von Schéele, F., and Nordh, L.: The OSIRIS instrument on the Odin spacecraft, *Can. J. Phys.*, 82, 411–422, 2004.

Liu, A. Z.: Estimate eddy diffusion coefficients from gravity wave vertical momentum and heat fluxes, *Geophys. Res. Lett.*, 36, L08806, doi:10.1029/2009GL037495, 2009.

**Water vapour and
the equatorial MSAO**

R. L. Gattinger et al.

Title Page

Abstract

Introduction

Conclusions

References

Tables

Figures

◀

▶

◀

▶

Back

Close

Full Screen / Esc

Printer-friendly Version

Interactive Discussion



Lossow, S., Urban, J., Gumbel, J., Eriksson, P., and Murtagh, D.: Observations of the mesospheric semi-annual oscillation (MSAO) in water vapour by Odin/SMR, *Atmos. Chem. Phys.*, 8, 6527–6540, doi:10.5194/acp-8-6527-2008, 2008.

Marsh, D., Smith, A., and Noble, E.: Mesospheric ozone response to changes in water vapor, *J. Geophys. Res.*, 108, 4109, doi:10.1029/2002JD002705, 2003.

McCormack, J. P., Hoppel, K. W., and Siskind, D. E.: Parameterization of middle atmospheric water vapor photochemistry for high-altitude NWP and data assimilation, *Atmos. Chem. Phys.*, 8, 7519–7532, doi:10.5194/acp-8-7519-2008, 2008.

McDade, I. C., Murtagh, D. P., Greer, R. G. H., Dickinson, P. H. G., Witt, G., Stegman, J., Llewellyn, E. J., Thomas, L., and Jenkins, D. B.: ETON 2: quenching parameters for the proposed precursors of $O_2(b^1\Sigma_g^+)$ and $O(^1S)$ in the terrestrial nightglow, *Planet. Space Sci.*, 34, 789–800, 1986.

Murtagh, D. P., Frisk, U., Merino, F., Ridal, M., Jonsson, A., Stegman, J., Witt, G., Eriksson, P., Jiménez, C., Megie, G., de la Nöe, J., Ricaud, P., Baron, P., Pardo, J. R., Hauchcorne, A., Llewellyn, E. J., Degenstein, D. A., Gattinger, R. L., Lloyd, N. D., Evans, W. F. J., McDade, I. C., Haley, C. S., Sioris, C., von Savigny, C., Solheim, B. H., McConnell, J. C., Strong, K., Richardson, E. H., Leppelmeier, G. W., Kyrölä, E., Auvinen, H., and Oikarinen, L.: An overview of the Odin atmospheric mission, *Can. J. Phys.*, 80, 309–319, 2002.

Picone, J. M., Hedin, A. E., Drob, D. P., and Aikin, A. C.: NRL-MSISE-00 empirical model of the atmosphere: statistical comparisons and scientific issues, *J. Geophys. Res.*, 107, 1468, doi:10.1029/2002JA009430, 2002.

Portnyagin, Y. I., Solov'eva, T. V., Merzlyakov, E. G., Pogorel'tsev, A. I., and Savenkova, E. N.: Height–latitude structure of the vertical wind in the upper mesosphere and lower thermosphere (70–110 km), *J. Atmos. Ocean. Phys.*, 46, 85–94, doi:10.1134/S0001433810010123, 2010.

Qian, L., Solomon, S. C., and Kane, T. J.: Seasonal variation of thermospheric density and composition, *J. Geophys. Res.*, 114, A01312, doi:10.1029/2008JA013643, 2009.

Richter, J. H. and Garcia, R. R.: On the forcing of the mesospheric semi-annual oscillation in the whole atmosphere community climate model, *Geophys. Res. Lett.*, 33, L01806, doi:10.1029/2005GL024378, 2006.

Richter, J. H., Sassi, F., Garcia, R. R., Matthes, K., and Fischer, C. A.: Dynamics of the middle atmosphere as simulated by the whole atmosphere community climate model, version 3 (WACCM3), *J. Geophys. Res.*, 113, D08101, doi:10.1029/2007JD009269, 2008.

**Water vapour and
the equatorial MSAO**

R. L. Gattinger et al.

Title Page

Abstract

Introduction

Conclusions

References

Tables

Figures

◀

▶

◀

▶

Back

Close

Full Screen / Esc

Printer-friendly Version

Interactive Discussion



- Sander, S. P., Friedl, R. R., Abbatt, J. P. D., Barker, J. R., Burkholder, J. B., Golden, D. M., Kolb, C. E., Kurylo, M. J., Moortgat, G. K., Wine, P. H., Huie, R. E., and Orkin, V. L.: Chemical Kinetics and Photochemical Data for Use in Atmospheric Studies, JPL Publication 10-6, Evaluation Number 17, California Institute of Technology, Pasadena, CA, 2011.
- 5 Sasi, M. N. and Vijayan, L.: Turbulence characteristics in the tropical mesosphere as obtained by MST radar at Gadanki (13.5° N, 79.2° E), *Ann. Geophys.*, 19, 1019–1025, doi:10.5194/angeo-19-1019-2001, 2001.
- Shapiro, A. V., Rozanov, E., Shapiro, A. I., Wang, S., Egorova, T., Schmutz, W., and Peter, Th.: Signature of the 27-day solar rotation cycle in mesospheric OH and H₂O observed by the
10 Aura Microwave Limb Sounder, *Atmos. Chem. Phys.*, 12, 3181–3188, doi:10.5194/acp-12-3181-2012, 2012.
- Sharp, W. E. and Kita, D.: In situ measurement of atomic hydrogen in the upper mesosphere, *J. Geophys. Res.*, 92, 4319–4324, 1987.
- Sheese, P. E., McDade, I. C., Gattinger, R. L., and Llewellyn, E. J.: Atomic oxygen densities re-
15 trieved from optical spectrograph and infrared imaging system observations of O₂ A-band airglow emission in the mesosphere and lower thermosphere, *J. Geophys. Res.*, 116, D01303, doi:10.1029/2010JD014640, 2011.
- Shepherd, M. G., Liu, G., and Shepherd, G. G.: Mesospheric semiannual oscillation in temperature and nightglow emission, *J. Atmos. Solar Terr. Phys.*, 68, 379–389, 2006.
- 20 Skinner, W. R., Yee, J. H., Hays, P. B., and Burrage, M. D.: Seasonal and local time variations in the O(¹S) green line, O₂ atmospheric band and OH Meinel band emissions as measured by the high resolution doppler imager, *Adv. Space Res.*, 21, 835–841, 1998.
- Smith, A. K.: Physics and chemistry of the mesopause region, *J. Atmos. Solar Terr. Phys.*, 66, 839–857, 2004.
- 25 Smith, A. K. and Marsh, D. R.: Processes that account for the ozone maximum at the mesopause, *J. Geophys. Res.*, 110, D23305, doi:10.1029/2005JD006298, 2005.
- Smith, A. K., Marsh, D. R., Russell III, J. M., Mlynczak, M. G., Martin-Torres, F. J., and Kyrölä, E.: Satellite observations of high nighttime ozone at the equatorial mesopause, *J. Geophys. Res.*, 113, D17312, doi:10.1029/2008JD010066, 2008.
- 30 Smith, A. K., Marsh, D. R., Mlynczak, M. G., and Mast, J. C.: Temporal variations of atomic oxygen in the upper mesosphere from SABER, *J. Geophys. Res.*, 115, D18309, doi:10.1029/2009JD013434, 2010.

**Water vapour and
the equatorial MSAO**

R. L. Gattinger et al.

Title Page

Abstract

Introduction

Conclusions

References

Tables

Figures

◀

▶

◀

▶

Back

Close

Full Screen / Esc

Printer-friendly Version

Interactive Discussion



Sonnemann, G. R. and Körner, U.: Total hydrogen mixing ratio anomaly around the mesopause region, *J. Geophys. Res.*, 108, 4692, doi:10.1029/2002JD003015, 2003.

Thomas, R. J.: Seasonal ozone variations in the upper mesosphere, *J. Geophys. Res.*, 95, 7395–7401, 1990.

5 Thomas, R. J.: Atomic hydrogen and atomic oxygen density in the mesopause region: global and seasonal variations deduced from solar mesosphere explorer near-infrared emissions, *J. Geophys. Res.*, 95, 16457–16476, 1995.

Tian, F., Kasting, J. F., Liu, H.-L., and Roble, R. G.: Hydrodynamic planetary thermosphere model: 1. response of the Earth's thermosphere to extreme EUV conditions and the significance of adiabatic cooling, *J. Geophys. Res.*, 113, E05008, doi:10.1029/2007JE002946, 2008.

10 Van der Loo, M. P. J. and Groenenboom, G. C.: Theoretical transition probabilities for the OH Meinel system, *J. Chem. Phys.*, 126, 114314–114317, 2007.

15 Van der Loo, M. P. J. and Groenenboom, G. C.: Erratum: “Theoretical transition probabilities for the OH Meinel system” [*J. Chem. Phys.* 126, 114314, 2007], *J. Chem. Phys.*, 128, 159901-2, doi:10.1063/1.2899016, 2008.

Wu, Q., Ortland, D. A., Killeen, T. L., Roble, R. G., Hagan, M. E., Liu, H.-L., Solomon, S. C., Xu, J., Skinner, W. R., and Niciejewski, R. J.: Global distribution and interannual variations of mesospheric and lower thermospheric neutral wind diurnal tide: 1. migrating tide, *J. Geophys. Res.*, 113, A05309, doi:10.1029/2007JA012542, 2008.

20 Xu, J., Gao, H., Smith, A. K., and Zhu, Y.: Using TIMED/SABER nightglow observations to investigate hydroxyl emission mechanisms in the mesopause region, *J. Geophys. Res.*, 117, D02301, doi:10.1029/2011JD016342, 2012.

25 Yee, J.-H., Roble, R. G., Skinner, W. R., Burrage, M. D., and Hays, P. B.: Global simulations and observations of $O(^1S)$, $O_2(^1\Sigma)$ and OH mesospheric nightglow emissions, *J. Geophys. Res.*, 102, 19949–19968, 1997.

**Water vapour and
the equatorial MSAO**

R. L. Gattinger et al.

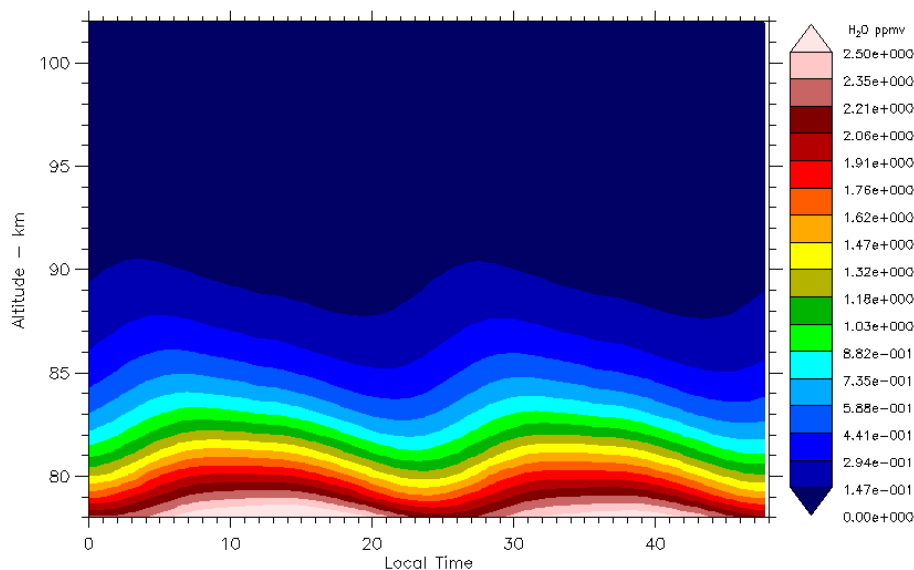


Fig. 1a. H₂O profiles for model days seven through eight for April equatorial conditions. The model initial conditions are from the ACE-FTS occultation measurements. The effect of the diurnal tide is apparent.

[Title Page](#)[Abstract](#)[Introduction](#)[Conclusions](#)[References](#)[Tables](#)[Figures](#)[◀](#)[▶](#)[◀](#)[▶](#)[Back](#)[Close](#)[Full Screen / Esc](#)[Printer-friendly Version](#)[Interactive Discussion](#)

**Water vapour and
the equatorial MSAO**

R. L. Gattinger et al.

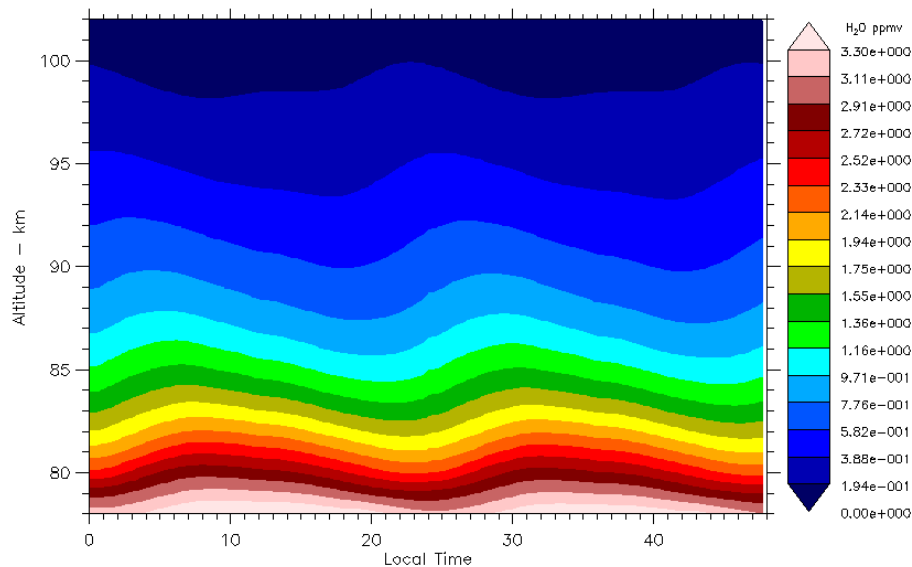


Fig. 1b. H₂O profiles for model days seven through eight for August equatorial conditions. Note the scale is 1.32 times larger than in (a). The August 90 km H₂O mixing ratio is approximately five times larger than for April.

[Title Page](#)[Abstract](#)[Introduction](#)[Conclusions](#)[References](#)[Tables](#)[Figures](#)[◀](#)[▶](#)[◀](#)[▶](#)[Back](#)[Close](#)[Full Screen / Esc](#)[Printer-friendly Version](#)[Interactive Discussion](#)

**Water vapour and
the equatorial MSAO**

R. L. Gattinger et al.

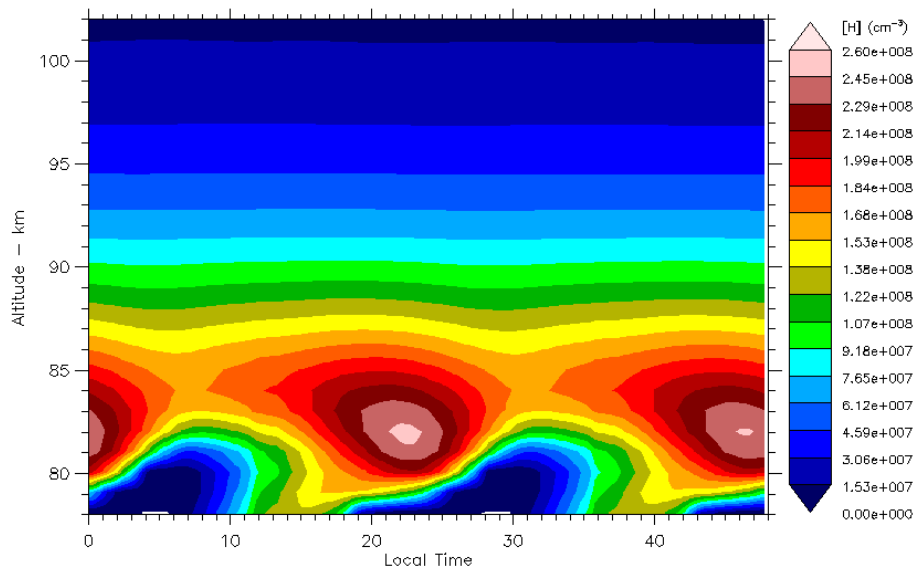


Fig. 2a. Simulated H for model days seven through eight for April at the equator. The dominant determining factors are the H₂O mixing ratio, from the ACE-FTS measurements, and the Lyman α flux from the SORCE dataset.

[Title Page](#)[Abstract](#)[Introduction](#)[Conclusions](#)[References](#)[Tables](#)[Figures](#)[◀](#)[▶](#)[◀](#)[▶](#)[Back](#)[Close](#)[Full Screen / Esc](#)[Printer-friendly Version](#)[Interactive Discussion](#)

**Water vapour and
the equatorial MSAO**

R. L. Gattinger et al.

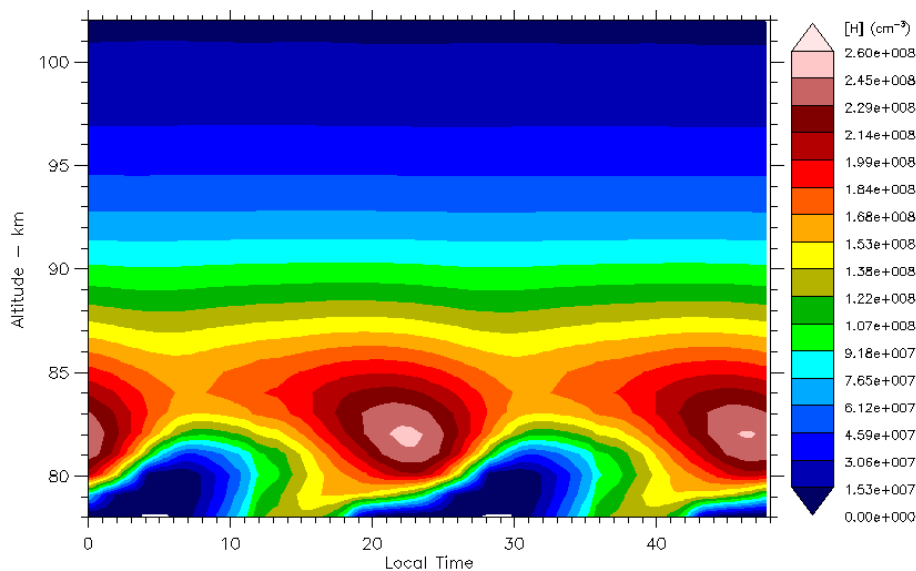


Fig. 2b. Model H for model days seven through eight for August at the equator. Note the scale is 1.12 times larger than in (a). From 85 to 90 km the April H values are approximately two-thirds the August values.

[Title Page](#)[Abstract](#)[Introduction](#)[Conclusions](#)[References](#)[Tables](#)[Figures](#)[◀](#)[▶](#)[◀](#)[▶](#)[Back](#)[Close](#)[Full Screen / Esc](#)[Printer-friendly Version](#)[Interactive Discussion](#)

**Water vapour and
the equatorial MSAO**

R. L. Gattinger et al.

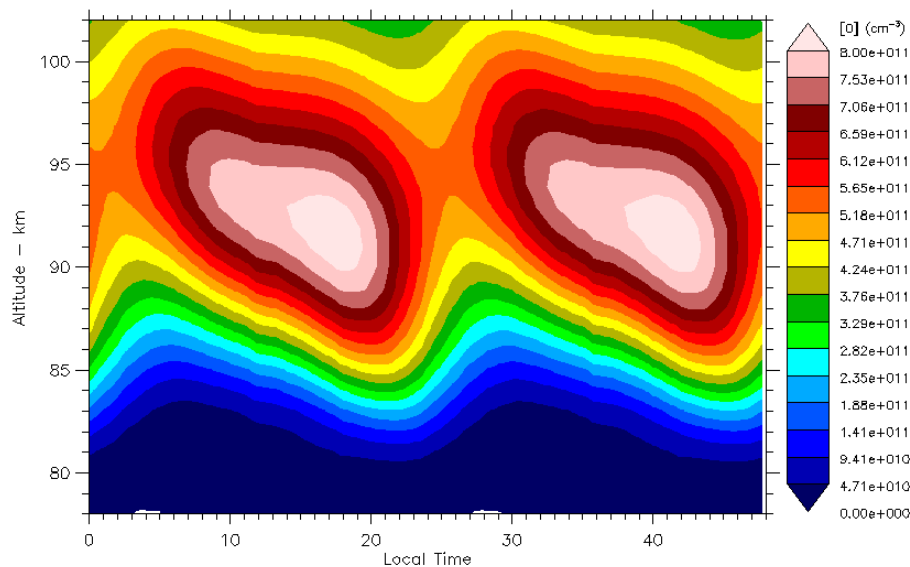


Fig. 3a. Local time variation of O for model days seven through eight in the April equatorial region. The effects of the diurnal tides are evident. The tidal phases compare well with the SABER O observations by Smith et al. (2010) and Shepherd et al. (2006).

[Title Page](#)[Abstract](#)[Introduction](#)[Conclusions](#)[References](#)[Tables](#)[Figures](#)[◀](#)[▶](#)[◀](#)[▶](#)[Back](#)[Close](#)[Full Screen / Esc](#)[Printer-friendly Version](#)[Interactive Discussion](#)

**Water vapour and
the equatorial MSAO**

R. L. Gattinger et al.

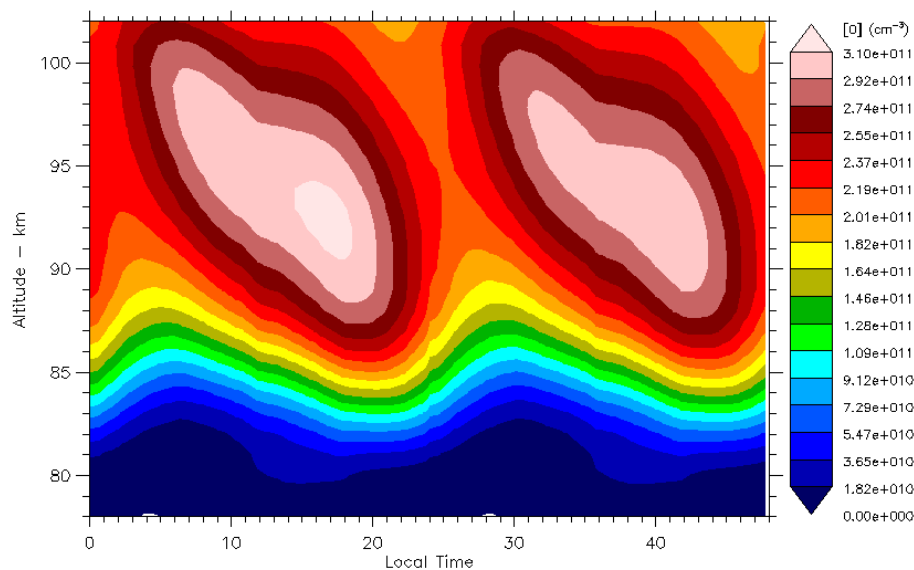


Fig. 3b. Local time variation of O for model days seven through eight in the equatorial region for August. The effects of the diurnal tides are again evident. Note the scale is 2.28 times smaller than in (a). The maximum O densities are less than one-half those for April in (a).

[Title Page](#)[Abstract](#)[Introduction](#)[Conclusions](#)[References](#)[Tables](#)[Figures](#)[◀](#)[▶](#)[◀](#)[▶](#)[Back](#)[Close](#)[Full Screen / Esc](#)[Printer-friendly Version](#)[Interactive Discussion](#)

**Water vapour and
the equatorial MSAO**

R. L. Gattinger et al.

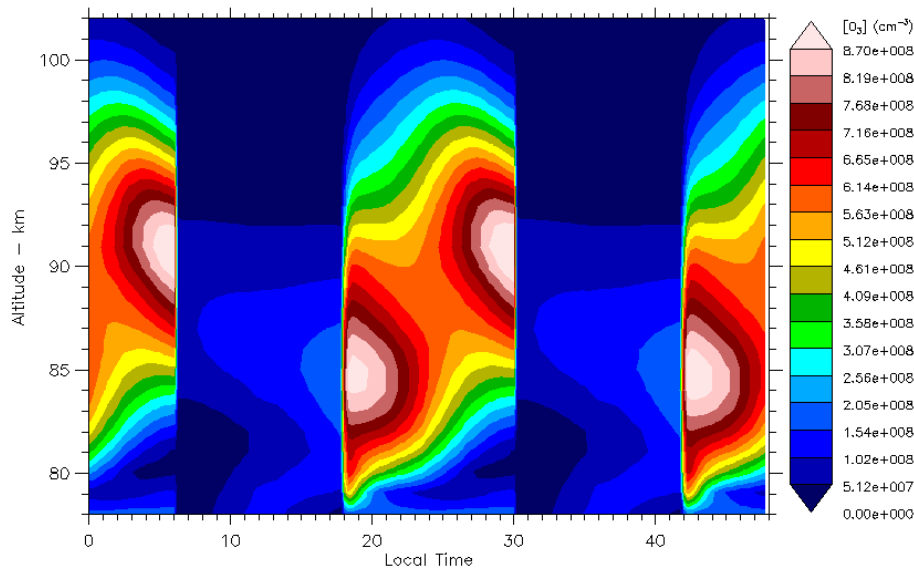


Fig. 4a. Local time variation of O_3 for model days seven through eight in the equatorial region for April. The effects of the diurnal tides are again evident. The large increase in O_3 just before sunrise is co-located with the diurnal temperature minimum and indicates the change in the O and O_3 partitioning with temperature.

[Title Page](#)[Abstract](#)[Introduction](#)[Conclusions](#)[References](#)[Tables](#)[Figures](#)[◀](#)[▶](#)[◀](#)[▶](#)[Back](#)[Close](#)[Full Screen / Esc](#)[Printer-friendly Version](#)[Interactive Discussion](#)

**Water vapour and
the equatorial MSAO**

R. L. Gattinger et al.

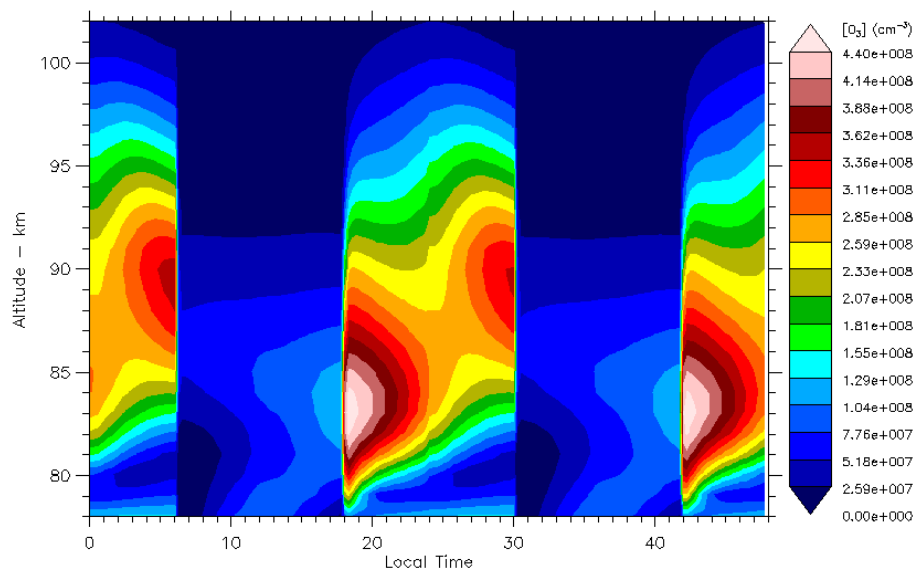


Fig. 4b. Local time variation of O_3 for model days seven through eight in the equatorial region for August. The effects of the diurnal tides are again evident. Note the scale is 1.98 times smaller than in (a). The August O_3 densities are approximately one-third the April densities.

[Title Page](#)[Abstract](#)[Introduction](#)[Conclusions](#)[References](#)[Tables](#)[Figures](#)[◀](#)[▶](#)[◀](#)[▶](#)[Back](#)[Close](#)[Full Screen / Esc](#)[Printer-friendly Version](#)[Interactive Discussion](#)

**Water vapour and
the equatorial MSAO**

R. L. Gattinger et al.

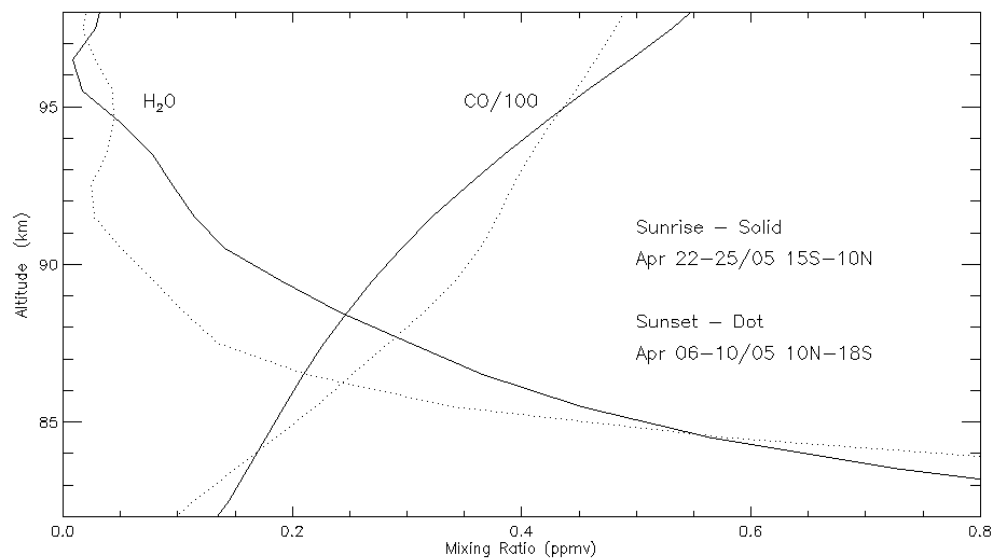


Fig. 5a. ACE-FTS mixing ratio observations for April 2005 sunrise and sunset at the equator showing the effects of the diurnal tides on CO and H₂O. The tides are out of phase, as expected, since the changes in mixing ratio profiles with altitude are of opposite sign.

[Title Page](#)[Abstract](#)[Introduction](#)[Conclusions](#)[References](#)[Tables](#)[Figures](#)[◀](#)[▶](#)[◀](#)[▶](#)[Back](#)[Close](#)[Full Screen / Esc](#)[Printer-friendly Version](#)[Interactive Discussion](#)

Water vapour and
the equatorial MSAO

R. L. Gattinger et al.

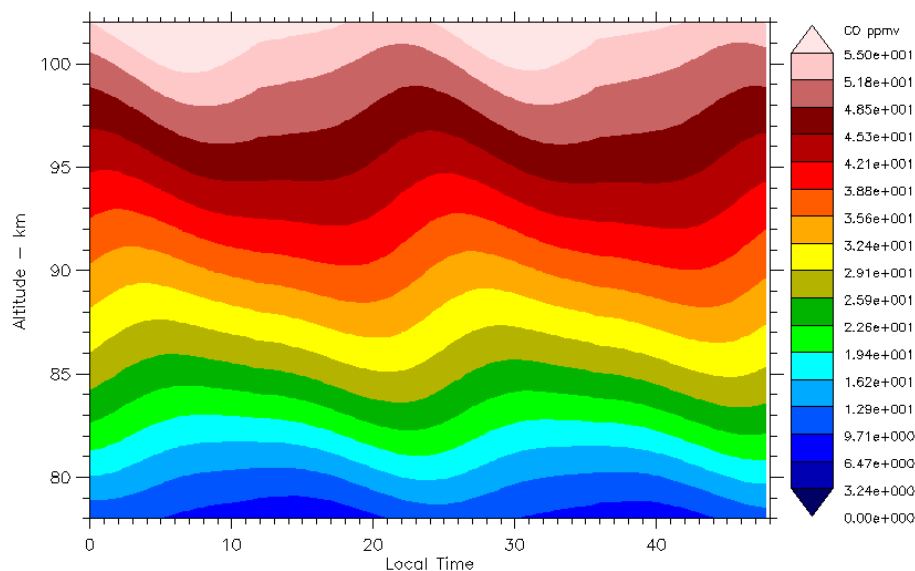


Fig. 5b. Model diurnal tide for CO for April, days seven through eight, for comparison with the ACE-FTS sunrise/sunset observations. At 90 km altitude the sunrise mixing ratio is smaller than the sunset mixing ratio, as in (a).

[Title Page](#)[Abstract](#)[Introduction](#)[Conclusions](#)[References](#)[Tables](#)[Figures](#)[◀](#)[▶](#)[◀](#)[▶](#)[Back](#)[Close](#)[Full Screen / Esc](#)[Printer-friendly Version](#)[Interactive Discussion](#)

Water vapour and the equatorial MSAO

R. L. Gattinger et al.

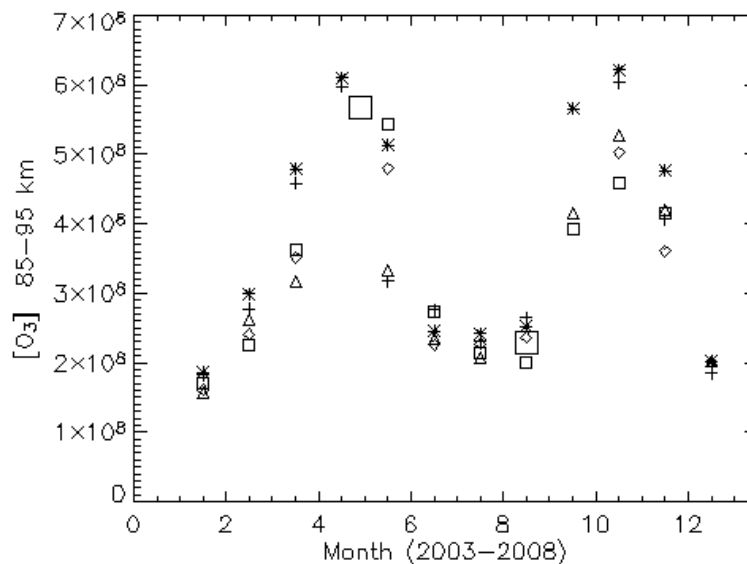


Fig. 6. The mesospheric semi-annual oscillation of O_3 density observed by the GOMOS instrument for night-time conditions is shown. Monthly averages are included where available for years from 2003 to 2008. The two large squares indicate the model O_3 densities for April “near equinox” and August “near solstice” conditions for approximately 23 H local time with baseline eddy mixing and background vertical winds.

Title Page

Abstract

Introduction

Conclusions

References

Tables

Figures

◀

▶

◀

▶

Back

Close

Full Screen / Esc

Printer-friendly Version

Interactive Discussion



Water vapour and
the equatorial MSAO

R. L. Gattinger et al.

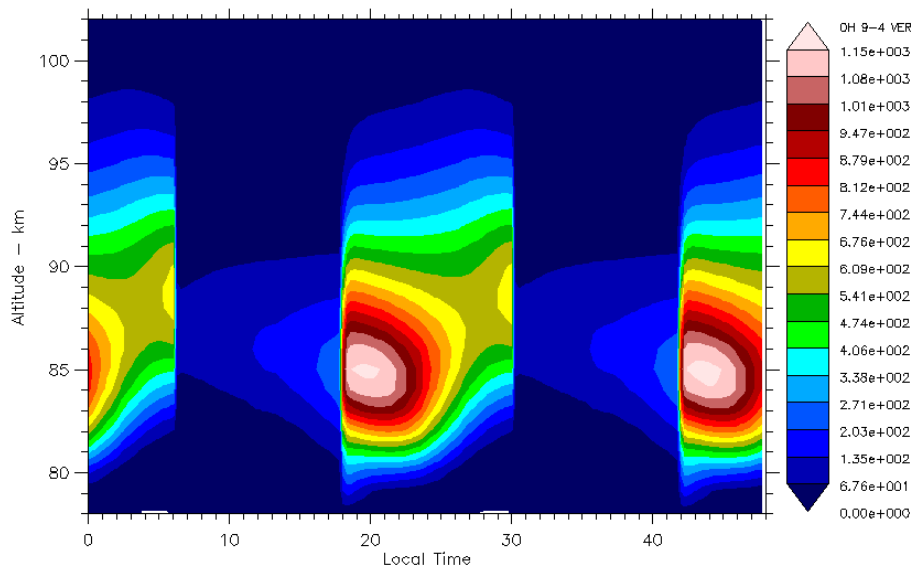


Fig. 7a. Model OH* 9-4 volume emission rates for April, days seven through eight, from model $[O_3]$ and $[H]$ values. Rates are from Adler-Golden (1997).

[Title Page](#)[Abstract](#)[Introduction](#)[Conclusions](#)[References](#)[Tables](#)[Figures](#)[I◀](#)[▶I](#)[◀](#)[▶](#)[Back](#)[Close](#)[Full Screen / Esc](#)[Printer-friendly Version](#)[Interactive Discussion](#)

Water vapour and
the equatorial MSAO

R. L. Gattinger et al.

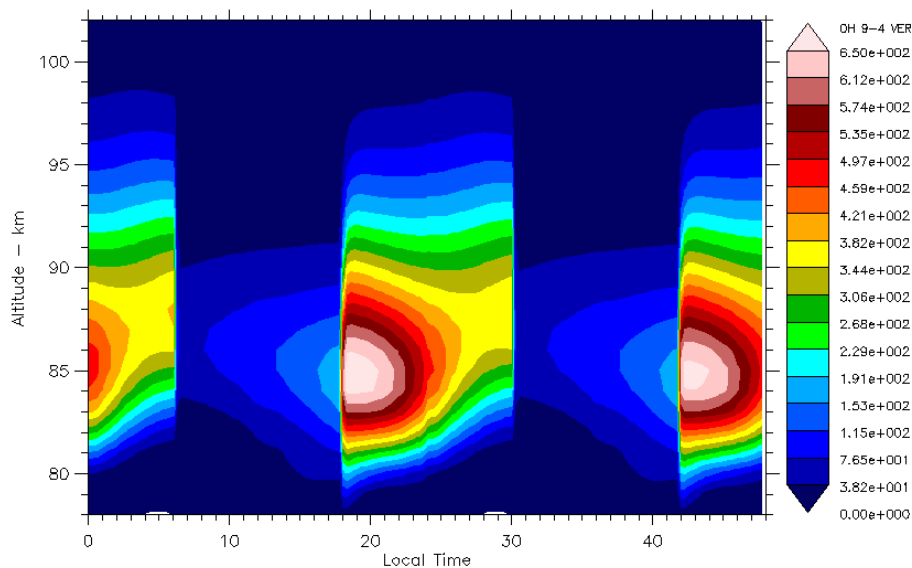


Fig. 7b. Model OH* 9-4 volume emission rates for August, days seven through eight, from model $[O_3]$ and $[H]$ values. Note the scale is 1.77 times smaller than in (a).

Title Page

Abstract

Introduction

Conclusions

References

Tables

Figures

◀

▶

◀

▶

Back

Close

Full Screen / Esc

Printer-friendly Version

Interactive Discussion



**Water vapour and
the equatorial MSAO**

R. L. Gattinger et al.

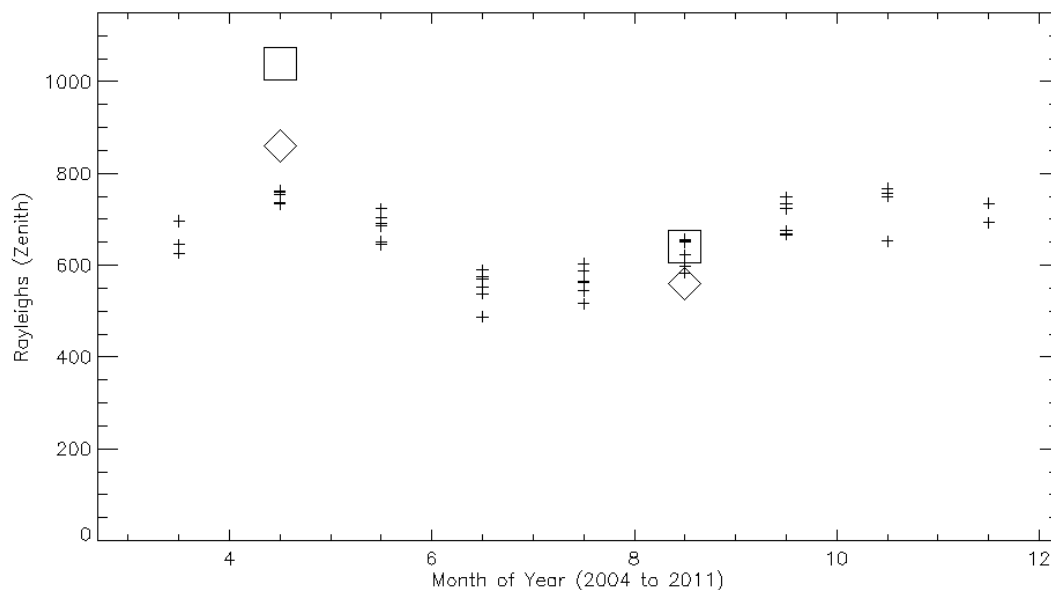


Fig. 8. Monthly averages of the OH* 9-4 brightness, referred to zenith viewing, as observed by OSIRIS in the equatorial region from 2004 to 2011 (plus signs). The April and August model OH* 9-4 brightness with rates from Adler-Golden (1997) are given by the square symbols. The diamond symbols are with the rate for OH* ($\nu' = 9$) removal by O arbitrarily scaled up by 3, near gas kinetic.

[Title Page](#)[Abstract](#)[Introduction](#)[Conclusions](#)[References](#)[Tables](#)[Figures](#)[◀](#)[▶](#)[◀](#)[▶](#)[Back](#)[Close](#)[Full Screen / Esc](#)[Printer-friendly Version](#)[Interactive Discussion](#)

Water vapour and the equatorial MSAO

R. L. Gattinger et al.

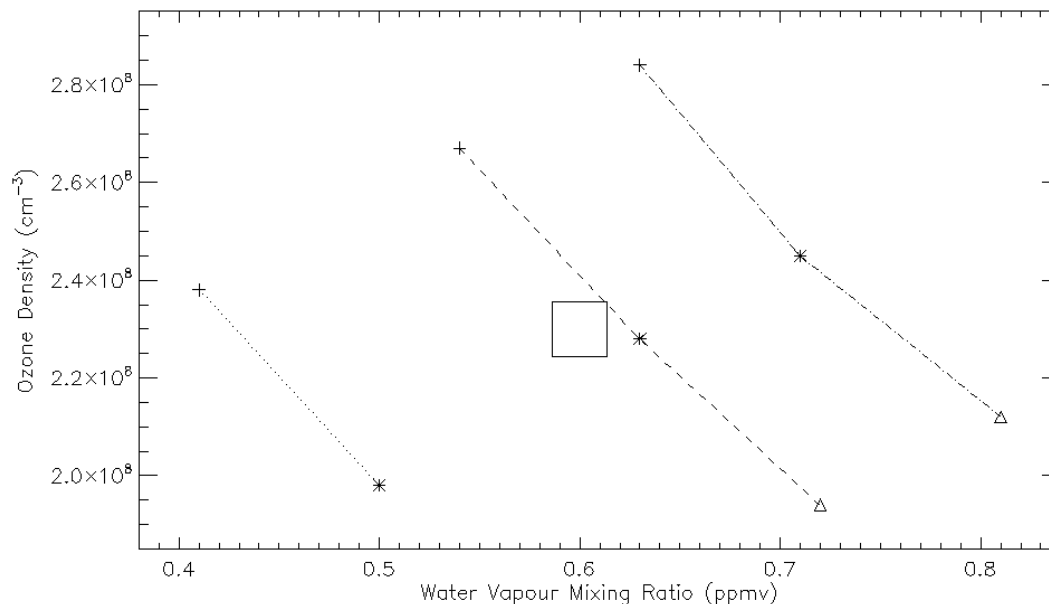


Fig. 9. The relationship between the combined effects of assumed eddy mixing rates and vertical advection and the model O_3 density and H_2O mixing ratio at an altitude of 90 km in August. The large square locates approximately the H_2O mixing ratio measured by ACE-FTS and the O_3 density measured by GOMOS. The plus signs are for an assumed vertical advection of 0.6 cm s^{-1} , the asterisks for 0.8 cm s^{-1} and the triangles for 1.0 cm s^{-1} . The dotted line is for an assumed eddy mixing of approximately $5 \times 10^5 \text{ cm}^2 \text{ s}^{-1}$, the dashed line for $1.0 \times 10^6 \text{ cm}^2 \text{ s}^{-1}$ and the dot-dash line for $2 \times 10^6 \text{ cm}^2 \text{ s}^{-1}$.

Title Page

Abstract

Introduction

Conclusions

References

Tables

Figures

◀

▶

◀

▶

Back

Close

Full Screen / Esc

Printer-friendly Version

Interactive Discussion

